Anomalous Hall and Nernst Effects in Co_2TiSn and $Co_2Ti_{0.6}V_{0.4}Sn$ Heusler Thin Films

Junfeng Hu,[1,2,*] Benedikt Ernst,[3,*] Sa Tu,[1,2,*] Marko Kuveždić,[4,*] Amir Hamzić,[4,1,*] Emil Tafra,[4]
Mario Basletić,[4] Youguang Zhang,[1] Anastasios Markou,[3] Claudia Felser,[3,†] Albert Fert,[5,1]
Weisheng Zhao,[1,‡] Jean-Philippe Ansermet,[2] and Haiming Yu[1,§]

[1] *Fert Beijing Institute, BDBC, School of Electronic and Information Engineering,Beihang University, Xueyuan Road 37, Beijing 100191, China*

[2] *Institute of Physics, Station 3, Ecole Polytechnique Fédérale de Lausanne, 1015 Lausanne, Switzerland*

[3] *Max Planck Institute for Chemical Physics of Solids, Nöthnitzer Strae 40, 01187 Dresden, Germany*

[4] *Department of Physics, Faculty of Science, University of Zagreb, Zagreb HR-10001, Croatia*

[5] *Unité Mixte de Physique CNRS, Thales, Université Paris-Sud, Université Paris-Saclay, 91767 Palaiseau, France*

Magnetotransport (magnetoresistance and anomalous Hall effect) and thermoelectric (Seebeck and anomalous Nernst effect) effects are investigated on epitaxially grown Co_2TiSn and $Co_2Ti_{0.6}V_{0.4}Sn$ Heusler thin films. An anomalous Nernst coefficient up to 1.8 $\mu V/K$ is observed in $Co_2Ti_{0.6}V_{0.4}Sn$ at 220 K, which is almost 12 times larger than in the undoped Co_2TiSn thin film at 300 K. In analogy to the anomalous Hall angle, we extract the anomalous Nernst angle from experimental results by comparing the anomalous Nernst voltage with the thermopower. The anomalous Nernst angle for $Co_2Ti_{0.6}V_{0.4}Sn$ is 15% at 220 K, whereas it is only 0.5% for the undoped film. Considering the Mott relation for anomalous Hall and Nernst effects, these experimental results may be accounted for by an enhanced energy derivative of the anomalous Hall conductivity at the Fermi level that is shifted by vanadium doping. These results of a large anomalous Nernst angle provide opportunities to realize spin-caloritronic devices for efficient on-chip energy harvesting based on magnetic Heusler thin films.

I. INTRODUCTION

The field of spintronics has been constantly searching for materials with large spin polarizations. Cobalt-based Heusler compounds such as Co_2XY (X = Ti, V, Mn, or Fe; Y = Al, Si, Ge, or Sn) [1–8] offer an ideal playground for spintronics since some of them are predicted to be half-metallic ferromagnets [9] with full spin polarization at the Fermi surface. Among the half-metallic Heusler compounds, Co_2MnSi has been demonstrated as a useful material for applications in spintronic devices because of the experimental observation of a large spin polarization [10]. Another possible system is Co_2TiSn (CTS), with high current spin polarization (0.64 ± 0.02) [11].

Over the last decade, thermoelectric effects have also been investigated on Heusler alloys; for instance the Seebeck effect (SE) [12], spin Seebeck effect (SSE) [13], and anomalous Nernst effect (ANE) [14]. The Nernst effect [15] is a magnetothermoelectric effect that has been known for more than a century. The ANE can be considered as the thermoelectric counterpart of the anomalous Hall effect (AHE). The ANE is found to dominate over the SSE [16,17] in many systems [14,18,19]. Other spin-dependent thermoelectric effects have been investigated [20–25] and contribute to the field of spin caloritronics [26,27]. The ANE has attracted increasing attention recently in different systems [14,18,28–35].

The relation between conductivity and thermoelectric conductivity is given by the Mott formula [36–38]. The relation between the anomalous Hall conductivity and anomalous Nernst conductivity has been studied in different systems, such as $CuCr_2Se_{4-x}Br_x$ [39] and $Ga_{1-x}Mn_xAs$ [40]. The Heusler compound CTS has attracted much attention as a potential candidate for spintronics applications [41]. We find by doping with vanadium its electric transport and particularly thermoelectric properties can be affected. A similar influence of doping has been investigated in other materials, such as (Ga,Mn)As [42] and $Bi_2Te_{3-x}Se_x$ [43].

We study the magnetic Heusler compounds CTS and $Co_2Ti_{0.6}V_{0.4}Sn$ (CTVS). This choice of compounds

---

*These authors contributed equally to this work.

†claudia.felser@cpfs.mpg.de

‡weisheng.zhao@buaa.edu.cn

§haiming.yu@buaa.edu.cn

follows the theoretical proposition of Wang *et al.* [44] that Co-based Heusler compounds Co_2YZ (with Co_2TiSn being one of them), with the number of valence electrons $N_v = 26$, would be candidates for Weyl metals, as well as systems with $N_v = 27$ (such as Co_2VSn). Co_2VSn is not a half-metallic ferromagnet, and in contrast to other Co-based Heusler compounds, its Curie temperature and magnetic moment deviate from linear (i.e., Slater-Pauling) variation as a function of N_v [45]. However, Co_2VSn has the same crystal structure as and one more electron per unit cell than Co_2TiSn; Wang *et al.* [44] calculated that doping Co_2TiSn with 10% V in the Ti site (and taking into account the disorder effects) would bring the Weyl points to the Fermi level while keeping the main band topology unchanged. This suggestion is also based on the results for the hyperfine fields for a series of $Co_2Ti_{1-x}V_xSn$ compounds, where it was found that increase of the conduction-electron density in $Co_2Ti_{1-x}V_xSn$ for $x < 0.6$ slightly increases the positive Sn hyperfine field (with a weak maximum at $x = 0.4$), and at higher V concentrations the values of the field are drastically reduced [46]. The same work showed that the magnetic moment remained relatively constant for $x \leq 0.8$ and decreased dramatically for $x = 1.0$.

II. MEASUREMENTS OF MAGNETOTRANSPORT AND THERMOELECTRIC PROPERTIES

We study the magnetotransport [resistivity, magnetoresistance (MR), and AHE] and thermoelectric (Seebeck and ANE) properties of magnetic Heusler compounds with and without vanadium (V) doping. Thin films of Co_2TiSn are grown on polished MgO(001) substrates by epitaxial growth from elementary Co, Ti, Sn, and V targets. All films are capped with 2–3 nm of aluminum at room temperature to prevent oxidation. We first pattern the sample into a stipe (9 mm long and 2 mm wide) with photolithography and argon-ion-beam etching. Then the gold electrodes of Cr(3 nm)/Au(100 nm) are deposited by electron-beam evaporation with photolithography and lift-off. The thickness of the samples is calculated from the deposition speed and time and are also measured by atomic force microscopy during the fabrication.

A. Magnetoresistance measurements

Low-temperature magnetometry is performed with a superconducting quantum-interference device to investigate the field dependence of the magnetization and to determine the Curie temperatures of the compounds. The Curie temperatures T_C are determined by the temperature dependence of the magnetization measured in a small induction field of 50 mT. The temperature dependence of the magnetization between 20 and 400 K is shown in Figs. 1(a) and 1(b) for CTS and CTVS. The Curie temperature of CTVS is approximately 280 K. All measurements performed on this compound are done at 220
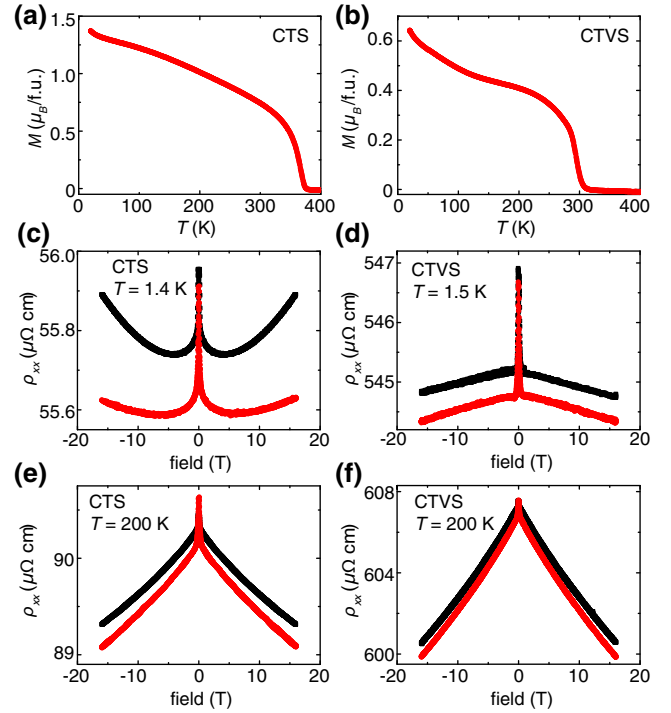

FIG. 1. Magnetization as a function of temperature for (a) Co_2TiSn and (b) $Co_2Ti_{0.6}V_{0.4}Sn$. Measurements are taken as a temperature sweep with a fixed field of 0.05 T. Magnetoresistance for Co_2TiSn and $Co_2Ti_{0.6}V_{0.4}Sn$ with the field in the out-of-plane direction (perpendicular magnetoresistance, black) and along the current direction (longitudinal magnetoresistance, red). (c),(e) The magnetoresistance for Co_2TiSn at 1.5 and 200 K. (d),(f) The magnetoresistance for $Co_2Ti_{0.6}V_{0.4}Sn$ at 1.5 and 200 K.

K, unless otherwise specified. One can also observe that the magnetization of CTVS starts increasing sharply when the temperature decreases below 125 K, and this is not understood so far. The Curie temperature of CTS is 360 K, which makes it possible to perform experiments at room temperature. It has been observed that T_C of CTS decreases with increasing disorder [41]. Hence the lower T_C of CTVS compared with CTS suggests that the V doping increases the disorder. One expects that partial replacement of Ti with V in an otherwise-stoichiometrically-ordered alloy would lead to a chemical disorder and this would manifest itself as expected in the increased resistivity values.

Magnetotransport properties are measured with an ac setup in a standard cryostat with magnetic fields up to 16 T, and in the temperature range between 1.5 and 300 K. In all measurements, the current direction is along the x axis (namely, in the direction of the sample length); the magnetic field is along the z axis (out of plane) for perpendicular magnetoresistance and along the x direction for longitudinal magnetoresistance. Some data are also obtained for a magnetic field along the y axis for in-plane perpendicular magnetoresistance (i.e., transverse magnetoresistance) and are presented in Fig. 2(b).
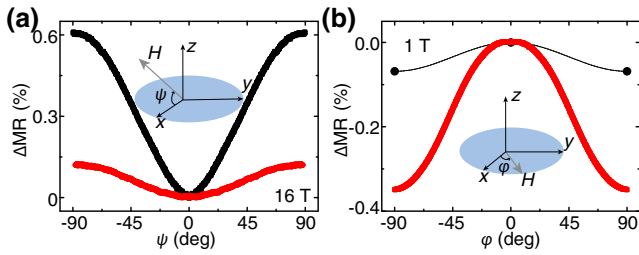
FIG. 2. (a) Magnetoresistance of Co_2TiSn and $Co_2Ti_{0.6}V_{0.4}Sn$ with the magnetic field (16 T) rotated from the out-of-plane z direction to the in-plane x direction at 200 K. (b) Magnetoresistance with the magnetic field (1 T) rotated in plane at 1.4 K for Co_2TiSn and 1.5 K for $Co_2Ti_{0.6}V_{0.4}Sn$. The dashed line is the cosine fit. The data are normalized to zero at $0°$. Co_2TiSn and $Co_2Ti_{0.6}V_{0.4}Sn$ are shown as black and red curves, respectively.

Normally, the MR of a ferromagnetic alloy includes a spontaneous contribution and a forced contribution at higher fields due to the progressive freezing and reduction of the spin-disorder resistance. These two mechanisms can be readily distinguished in the data in Figs. 1(c)–1(f). One can also notice for CTS the appearance of a positive normal MR at 1.4 K [see Fig. 1(c)]. However, with increasing temperature, the negative high-field MR quickly becomes much larger and a dominating contribution [see Fig. 1(e)]. CTVS always shows a negative MR at both temperatures, but again it is much larger at high temperature [see Figs. 1(d) and 1(f)]. Overall, the MR is small (less than 1%) and of the same order as in a single crystal of Ni [47]. Our observation is consistent with another study of epitaxial CTS thin films [4].

Moreover, the anisotropy effects are without any significant deviation (see Fig. 2). The angle dependence of magnetotransport properties is measured in the cryostat, where the sample holder can be rotated both in plane and out of plane. We perform angle scan measurements in the xz plane from $-90°$ to $+90°$ at 200 K, with magnetic field fixed at 16 T, on both compounds. The results are shown in Fig. 2(a). Here, the current direction is along the x axis; the magnetic field along the z axis is defined to be $\pm90°$ and that along the x axis is defined to be $0°$.

In addition, we also perform measurements with a 1-T magnetic field rotated in the xy plane ($0°$ is defined as when the field is along the current direction; namely, the x axis.). A very clear cosine-like variation with π periodicity can been seen for $Co_2Ti_{0.6}V_{0.4}Sn$ at 1.5 K in Fig. 2(b). For Co_2TiSn we have MR data for only $0°$ and $\pm90°$, which we also fit to cosine variation (dashed line). To sum up, the experimental results show very small MR in all configurations, and we believe that there is no significant deviation from the classical cosine-like variation that is associated with the so-called anisotropic magnetoresistance effect.
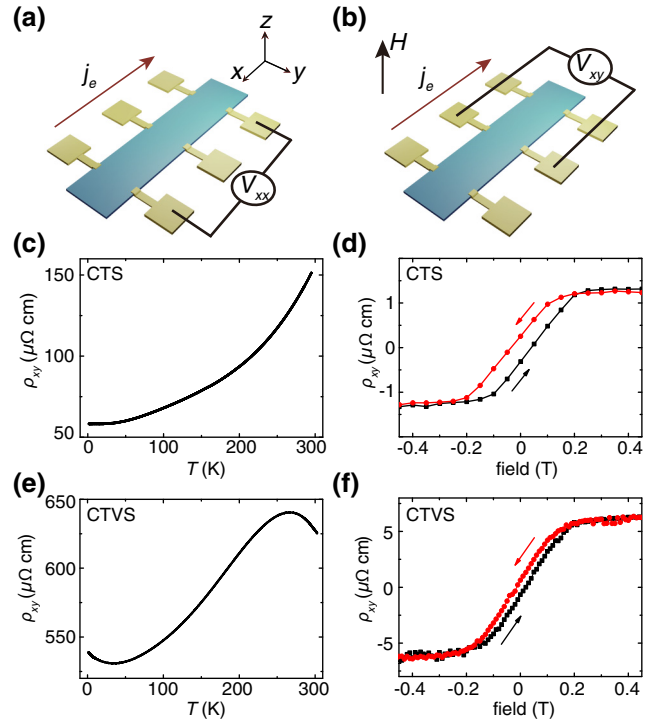

FIG. 3. (a),(b) Setups for measurement of resistance and the anomalous Hall effect, respectively. Resistivity as a function of temperature from 1.4 to 300 K for (c) Co_2TiSn and (e) $Co_2Ti_{0.6}V_{0.4}Sn$. Anomalous Hall resistivity as a function of magnetic field for (d) Co_2TiSn at 300 K and (f) $Co_2Ti_{0.6}V_{0.4}Sn$ at 220 K.

B. Anomalous Hall effect

Schematics for the resistivity measurement and for the AHE measurement are shown in Figs. 3(a) and 3(b), respectively. Figure 3(c) shows the temperature dependence of the resistivity of CTS from 1.4 to 300 K; it exhibits metallic behavior. This temperature dependence is consistent with that of bulk CTS [4]. However, the resistivity is lower for our thin films than for the bulk samples, but is similar to the values found by others using thin films [41]. The fact that the residual resistivities for both thin-film samples are smaller than for the bulk samples [4] indicates that both thin films have good crystallinity and chemical ordering.

The presence of chemical disorder is clearly indicated by the temperature-dependent resistivity measurement on the CTVS sample [see Fig. 3(e)]: its resistivity values are several times higher, and at low T (around 35 K) one clearly observes a minimum; similar characteristics are also seen in a nonannealed sample in Ref. [41] and in some other Heusler systems [7].

In Fig. 3(e), the resistivity for CTVS increases with temperature and reaches a maximum around the Curie temperature T_C (280 K). Also, with decreasing temperature, the resistivity increases again near our measurement
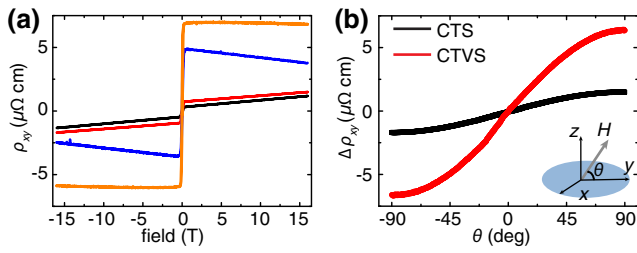
FIG. 4. Anomalous-Hall-effect measurements at a magnetic field of up to 16 T. (a) Field dependence of Hall resistivity. The black and red curves represent Co_2TiSn at 1.4 and 200 K, while blue and orange curves represent $Co_2Ti_{0.6}V_{0.4}Sn$ at 1.5 and 200 K, respectively. (b) Angle dependence of Hall resistivity while the samples are rotated in the yz plane for Co_2TiSn at 1.5 K and $Co_2Ti_{0.6}V_{0.4}Sn$ at 200 K.

limit; namely, 1.5 K. This pronounced anomaly of the resistivity at the the Curie temperature has also been observed in bulk samples of Co_2TiSn, and is associated with the ferromagnetic-to-paramagnetic transition [3,4,48]. Changes in the behavior of the resistivity at the the Curie temperature are well known for the ferromagnetic metals Ni [49] and Fe [50]. A similar change was recently reported for Co_2TiAl [51], a compound that is closely related to the Co_2TiSn compounds investigated here. Besides the anomaly in magnetic-scattering resistivity, these papers pointed out that changes in the electronic structure at the phase transition may also give rise to changes in the temperature dependence of the resistivity. The resistivity anomaly at lower temperatures (approximately 35 K) is more likely to be related to chemical disorder, as discussed by Hazra *et al.* [7]

The low-field AHE contribution of CTS [see Fig. 3(d)] is of the same order of magnitude as in Ref. [41]. The low-field AHE resistivity of CTVS [see Fig. 3(f)] is much bigger, due to the disorder induced by V doping. The AHE is also investigated at 1.4 K (1.5 K) and 200 K with a field up to 16 T (see Fig. 4). From high-field parts of the results shown in Fig. 4(a), different type of carriers can be distinguished from Co_2TiSn and $Co_2Ti_{0.6}V_{0.4}Sn$; namely, the carriers in Co_2TiSn are holes (form the positive slope of the ordinary Hall effect) and in $Co_2Ti_{0.6}V_{0.4}Sn$ are electrons (from the negative slope of the ordinary Hall effect), and the corresponding number of carriers at high temperatures is 3 times greater than in CTS. The angle dependence of anomalous Hall resistivity is also investigated in these two films while the samples are rotated form in plane to out of plane. The Hall resistivity ρ_{xy} has a sine-like variation with 2π periodicity, as shown in Fig. 4(b).

We now briefly discuss the physical model responsible for the AHE. It has been shown [52,53] that the AHE can be accounted for by several models based on the intrinsic (interband effect and the Berry phase) and extrinsic (skew-scattering and side-jump effect) mechanisms, which dominate in a particular conductivity regime, and

which are characterized by a specific power-law relationship between the anomalous Hall resistivity ρ_{xy} and the longitudinal resistivity ρ_{xx}. For pure metals and at low temperatures, the major contribution is due to the skew scattering (and $\rho_{xy} \approx \rho_{xx}$), while in alloys or disordered materials with large resistivity, the intrinsic and side-jump mechanisms give rise to the AHE with $\rho_{xy} \approx \rho_{xx}^2$. On the basis of values of their resistivity, the compounds investigated in this study belong to a "good-metal" (or moderate-conductivity) regime, where the intrinsic and side-jump mechanisms give rise to the AHE. (Although the measurements are performed at only a few temperatures, yielding a limited number of experimental points, the $\log\rho_{xx}$ versus $\log\rho_{xy}$ plot confirms the theoretically predicted exponent $n = 2$.)

C. Anomalous Nernst effect and Seebeck effect

To conduct the thermoelectric measurements, we use a ceramic heater at one side of the sample with a copper sink at the other side to generate the temperature gradient. Two Pt thermometers are used to measure the temperature gradient between end sides of the sample. The anomalous Nernst voltage is measured on the Hall bar contacts as a function of the applied out-of-plane magnetic field while the in-plane temperature gradient is kept fixed [Fig. 5(a)]. Figures 5(c) and 5(e) show the ANE results for CTVS and CTS, respectively. In the saturated-magnetic-field range, CTVS shows an anomalous Nernst voltage V_{ANE} of up to 2.4 μV at 220 K, and it is more than 10 times larger than that of CTS at 300 K.

The anomalous Nernst voltage V_{ANE} induced by $\nabla_x T$ can be described by $V_{ANE} = -wN_{ANE}\nabla_x T$ [30]. With a fixed in-plane temperature gradient $\nabla_x T$ of 6.7 K/cm and 2-mm width w between the two voltage pads, one can determine the absolute anomalous Nernst coefficients $N_{CTVS} \approx 1.8$ μV/K at 220 K and $N_{CTS} \approx 0.15$ μV/K at 300 K.

The same setup is used to measure the Seebeck voltage as a function of the applied in-plane temperature difference [Fig. 5(b)]. The Seebeck voltages are measured for CTVS [Fig. 5(d)] and CTS [Fig. 5(f)]. The Seebeck coefficients extracted from the linear fitting relation of the data are $S_{CTVS} \approx -12$ μV/K at 220 K and $S_{CTS} \approx -30$ μV/K at 300 K based on $V_{SE} = S\Delta T$ (The reason why there is no minus is because the Seebeck voltage we measure here is between the cold side and the hot side.). This Seebeck coefficient of CTS is in a good agreement with the published data of Balke *et al.* [12].

III. ANOMALOUS HALL AND NERNST ANGLES

In the analysis of the AHE, the concept of the anomalous Hall angle [53,54] was introduced, which helps to understand the relation between the anomalous Hall resistivity (ρ_{xy}) and the normal resistivity (ρ_{xx}): $\theta_H = \rho_{xy}/\rho_{xx}$. [The anomalous Hall angle can also be defined
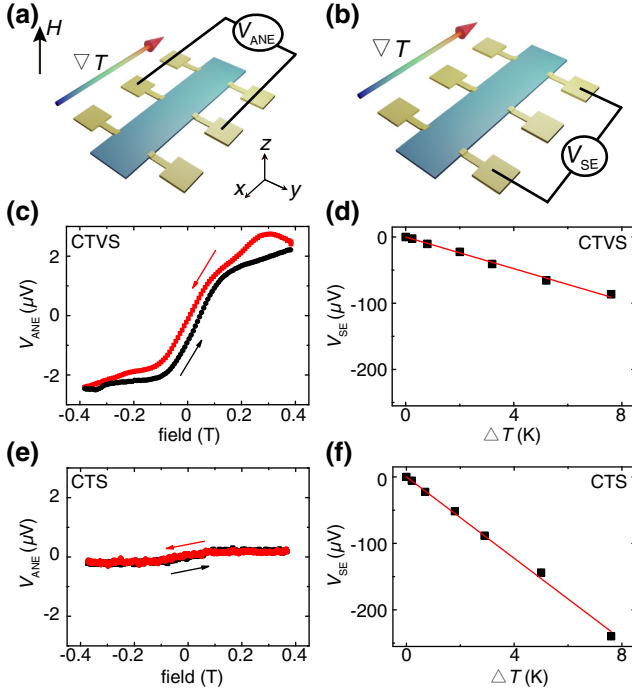
FIG. 5. (a),(d) Setup for measurement of the ANE and the Seebeck effect, respectively. The anomalous Nernst voltage as a function of magnetic field for (c) Co_2TiVSn at 220 K and (e) Co_2TiSn at 300 K with a fixed temperature gradient of 6.7 K/cm. The Seebeck voltage as a function of temperature difference for (d) Co_2TiVSn at 220 K and (f) Co_2TiSn at 300 K.

by electrical conductivity; namely, $\theta_H = -\sigma_{xy}/\sigma_{xx}$, where $\sigma_{xx} = \rho_{xx}/(\rho_{xx}^2 + \rho_{xy}^2)$ and $\sigma_{xy} = -\rho_{xy}/(\rho_{xx}^2 + \rho_{xy}^2)$.] This dimensionless parameter resulting from the AHE describes the deviation of the flow of electrons from the direction of the longitudinal electric field generated by the current, and indicates the conversion efficiency of the AHE.

Taking the data for ρ_{xy} and ρ_{xx} measured on the compounds (Fig. 3), we find that the anomalous Hall angles for CTS and CTVS are fairly similar (0.79% and 0.87%). The anomalous Hall angles are rarely found to be very large [53]: for thick NiFe films, they range from -0.2% to 0.1% [55] and for NiFe capped with a Pt layer, the values are enhanced by almost 1 order of magnitude [56]. We also note here the values for Co/Pt multilayers range from 1% to 2.5% with different thickness of Pt, and for ordered FePt evaporated film, the maximum value of the Hall angle is 1.2% [57]. Recently, Ikhlas *et al.* [35] measured the anomalous Hall angle to be 1% in a chiral antiferromagnet Mn_3Sn system.

In analogy to the anomalous Hall angle, we define the anomalous Nernst angle [34] θ_N as the ratio of the anomalous Nernst coefficient N and the Seebeck coefficient S; that is $\theta_N = N/S$. Similarly to anomalous Hall angle, the anomalous Nernst angle also indicates the conversion

efficiency between the ANE and the Seebeck effect. We extract the anomalous Nernst angle from the experimental data obtained with the Heusler thin films. The anomalous Hall and Nernst angles on CTVS and CTS are drastically different. CTVS exhibits a surprisingly large anomalous Nernst angle of up to 15%, which is 30 times larger than that of the undoped CTS, and 6 times larger than that of the chiral antiferromagnet Mn_3Sn (2.5%) recently studied by Ikhlas *et al.* [35].

These results reveal that anomalous Nernst and Hall angles are not simply proportional. The Mott relation [Eq. (1)] shows that the thermoelectric conductivity α_{xx} is related to the energy derivative of the electrical conductivity σ_{xx} at the Fermi level:

$$\alpha_{xx} = \frac{\pi^2 k_B^2 T}{3e}\sigma_{xx}'(\varepsilon_F). \quad (1)$$

If one assumes the Mott relation to be valid for anomalous transport, the anomalous Nernst conductivity α_{xy} can be written as [40,58,59]

$$\alpha_{xy} = \frac{\pi^2 k_B^2 T}{3e}\sigma_{xy}'(\varepsilon_F). \quad (2)$$

Considering $\tilde{\alpha} = \tilde{\sigma}\tilde{S}$, we can write the matrix as follows:

$$\begin{pmatrix} \alpha_{xx} & \alpha_{xy} \\ -\alpha_{xy} & \alpha_{xx} \end{pmatrix} = \begin{pmatrix} \sigma_{xx} & \sigma_{xy} \\ -\sigma_{xy} & \sigma_{xx} \end{pmatrix}\begin{pmatrix} S_{xx} & S_{xy} \\ -S_{xy} & S_{xx} \end{pmatrix}. \quad (3)$$

With Eq. (3), we can derive the Seebeck coefficient S and the Nernst coefficient N as

$$S = S_{xx} = \frac{\sigma_{xx}\alpha_{xx} + \sigma_{xy}\alpha_{xy}}{\sigma_{xx}^2 + \sigma_{xy}^2},$$

$$N = S_{xy} = \frac{\sigma_{xx}\alpha_{xy} - \sigma_{xy}\alpha_{xx}}{\sigma_{xx}^2 + \sigma_{xy}^2}. \quad (4)$$

Therefore, the anomalous Nernst angle can be simplified as

$$\theta_N = \frac{\alpha_N + \theta_H}{1 - \alpha_N\theta_H}, \quad (5)$$

where $\alpha_N = \alpha_{xy}/\alpha_{xx}$ is the Peltier angle [60]. The Nernst angle is slightly different but is related to the Peltier angle. The Peltier angle is more similar to the Hall angle since both of them are directly linked to the conductivity. However, the Nernst angle we define here is more practical and can be used to unambiguously describe the relation between the Nernst coefficient and the Seebeck coefficient from experiments.

When the experimental results show that the anomalous Nernst angle θ_N equals the anomalous Hall angle θ_H, we

can conclude that $\alpha_N \ll \theta_H$. Applying Mott's formula for $\tilde{\alpha}$, based on Eqs. (1) and (2), we can derive

$$\alpha_N = \frac{\sigma'_{xy}(\varepsilon_F)}{\sigma'_{xx}(\varepsilon_F)}. \qquad (6)$$

We can get $\sigma'_{xy}(\varepsilon_F)/\sigma'_{xx}(\varepsilon_F) \ll \sigma_{xy}/\sigma_{xx}$ (for the case of $\theta_N = \theta_H$). Since θ_H is small, this means that $\sigma'_{xy}(\varepsilon_F) \approx 0$, which could be the case for results obtained with CTS. However, CTVS the anomalous Nernst angle is much larger than the anomalous Hall angle. This observation indicates the assumption of $\alpha_N \ll \theta_H$ no longer holds. This suggests that the energy-derivative ratio $\sigma'_{xy}(\varepsilon_F)/\sigma'_{xx}(\varepsilon_F)$ may be the key influential factor that leads to the discrepancy between the anomalous Nernst and Hall angles observed in the experimental results.

For CTVS, the doping of vanadium might have moved the Fermi level (ε_F) [61,62], where a peak in the density of states occurs near ε_F [63]. This might result in a drastic change of the energy derivative of the anomalous Hall conductivity (while not simultaneously for the longitudinal conductivity) and therefore lead to a large anomalous Nernst angle as observed for CTVS, $\theta_N = 15\%$. The different behavior of the ANE between CTVS and CTS due to the different energy derivatives of conductivity at the Fermi level could be further explored by band-structure calculation of the density of states, which, however, is not done in the current work. On the basis of Eq. (5) and taking the experimental value of the anomalous Hall angle $\theta_H = 0.87\%$, one may derive $\alpha_N = \sigma'_{xy}(\varepsilon_F)/\sigma'_{xx}(\varepsilon_F) \approx 14\%$, and apparently this value is not negligible compared with θ_N. Further studies on samples with different doping densities could provide insightful understanding of the relations between the anomalous Nernst and Hall angles.

By the doping of CTS with vanadium, our results indicate that material engineering may lead to a large anomalous Nernst angle that can enhance the performance of thermoelectric devices based on the ANE. The ANE enjoys an innate advantage over the conventional Seebeck effect in that the detection orientation is transverse to the temperature gradient. Therefore, the accumulation of the ANE voltage can be realized simply that make the distance in between the voltage contaces longer. In Fig. 6, thermopile devices based on the anomalous Nernst effect are proposed.

Figure 6(a) [64] shows the meanderlike thermopile design for energy harvesting of the in-plane temperature gradient. The field is applied in the out-of-plane direction to saturate the magnetization in a perpendicular configuration. Multiple Heusler bars can be patterned by lithography. The ANE voltage can be enhanced several times with this meanderlike design with use of a nonmagnetic metal such as gold to connect the head and the end of the Heusler bars. If one takes advantage of cutting-edge electron-beam lithography, a nanostructured thermoelectric device [65] based on the ANE may enhance the ANE
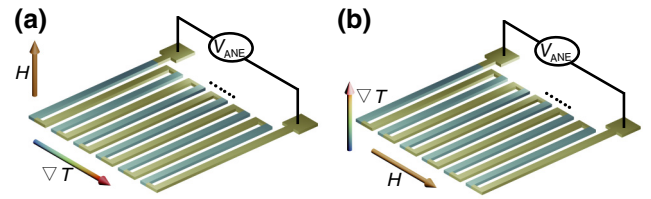

FIG. 6. The proposed thermopile based on the anomalous Nernst effect. Two different configurations of the design are shown: (a) in-plane temperature gradient and out-of-plane magnetic field; (b) out-of-plane temperature gradient and in-plane magnetic field. The blue bars are Heusler thin films and the yellow bars represent gold connecting leads.

voltage hundreds or even thousands of times. Furthermore, if the Heusler thin film can be grown with perpendicular magnetic anisotropy, similarly to the magnetic mulilayers used in a hard drive, one can replace gold lines with Heusler bars where the magnetizations of two adjacent Heusler bars are opposite, in other words, are in an antiparallel configuration [66]. In this case, the thermopile can also be turned on and off simply by switching the magnetizations of the neighboring Heusler bars between parallel and antiparallel configurations. Fig. 6(b) [35,66] shows the device with an in-plane magnetic field where energy harvesting from an out-of-plane temperature gradient can be envisaged. In a thin-film device, a large out-of-plane temperature gradient can be easily generated, such as by a laser shining on the top or heating from the bottom. This configuration is promising for device charging from the temperature difference between the human body and the external environment. With nanofabrication, one can easily obtain a voltage of up to 1 V in a 1-cm^2 wafer, which can be considered for sensors. If we use the Heusler alloy to make a single stripe line length of 1 cm and width of 300 nm connected to a same-sized copper stripe with a total size of about 1000 nm in width, we can make 1×10^4 periods in a 1×1 cm^2 chip. With a very small in-plane field and out-of-plane temperature difference of 0.1 mK over 10-nm thickness, the estimated voltage can increase to 1.8 V. This could be useful for applications such as an integrated thermopile in a ski suit to charge internet-of-things devices, for instance.

IV. CONCLUSION

We perform magnetoelectric and thermoelectric transport measurements on Co$_2$TiSn and Co$_2$Ti$_{0.6}$V$_{0.4}$Sn Heusler thin films. A reasonably large anomalous Hall conductivity in Co$_2$TiSn is observed. The Co$_2$Ti$_{0.6}$V$_{0.4}$Sn thin film showed a smaller anomalous Hall conductivity due to the disorder. Both compounds show a small and quasi-isotropic magnetoresistance. Anomalous Nernst measurements give very different results for CTS and CTVS. A large anomalous Nernst coefficient of up to 1.8 μV/K

is observed in $Co_2Ti_{0.6}V_{0.4}Sn$, more than 10 times larger than that of the undoped Co_2TiSn thin film. In particular, we compare the anomalous Hall and Nernst angles of these two compounds. While the anomalous Hall angles are fairly comparable, the anomalous Nernst angles exhibit large differences; namely, 15% for CTVS and 0.5% for CTS. If the Mott relations can presumably be applied also to the anomalous transport effects, the large difference of the anomalous Nernst angles may be explained as a result of the doping-induced Fermi-level shift that creates a sharp change of the energy derivative of the anomalous Hall conductivity. How the doping percentage affects the anomalous Nernst angle requires a systematic investigation with a series of doped Heusler thin-film samples. Further material engineering is expected to achieve an even larger anomalous Nernst angle. Finally, microstructured meanderlike spin-caloritronic devices are proposed to further increase the efficiency for on-chip energy harvesting based on magnetic Heusler thin films.

[1] J. Schmalhorst, M. D. Sacher, V. Höink, G. Reiss, A. Hütten, D. Engel, and A. Ehresmann, Magnetic and chemical properties of Co2MnSi thin films compared to the Co2MnSi/Al-O interface, J. Appl. Phys. **100**, 113903 (2006).

[2] H. C. Kandpal, G. H. Fecher, and C. Felser, Calculated electronic and magnetic properties of the half-metallic, transition metal based Heusler compounds, J. Phys. D: Appl. Phys. **40**, 1507 (2007).

[3] J. Barth, G. H. Fecher, B. Balke, S. Ouardi, T. Graf, C. Felser, A. Shkabko, A. Weidenkaff, P. Klaer, H. J. Elmers, H. Yoshikawa, S. Ueda, and K. Kobayashi, Itinerant half-metallic ferromagnets Co_2TiZ ($Z =$ Si, Ge, Sn): Ab initio calculations and measurement of the electronic structure and transport properties, Phys. Rev. B **81**, 064404 (2010).

[4] M. Meinert, J. Schmalhorst, H. Wulfmeier, G. Reiss, E. Arenholz, T. Graf, and C. Felser, Electronic structure of fully epitaxial Co_2TiSn thin films, Phys. Rev. B **83**, 064412 (2011).

[5] T. Graf, C. Felser, and S. S. P. Parkin, Simple rules for the understanding of Heusler compounds, Prog. Solid State Chem. **39**, 1 (2011).

[6] B. M. Ludbrook, B. J. Ruck, and S. Granville, Perpendicular magnetic anisotropy in $Co_2Fe_{0.4}Mn_{0.6}Si$, J. Appl. Phys. **120**, 013905 (2016).

[7] B. K. Hazra, M. M. Raja, R. R. Rawat, A. Lakhani, S. N. Kaul, and S. Srinath, Effect of disorder on the anomalous Hall conductivity of Co_2FeSi thin films, J. Magn. Magn. Mater. **448**, 371 (2018).

[8] J. Qiao, S. Peng, Y. Zhang, H. Yang, and W. Zhao, First-principles investigation of magnetocrystalline anisotropy oscillations in Co_2FeAl/Ta heterostructures, Phys. Rev. B **97**, 054420 (2018).

[9] R. A. de Groot, F. M. Mueller, P. G. van Engen, and K. H. J. Buschow, New Class of Materials: Half-Metallic Ferromagnets, Phys. Rev. Lett. **50**, 2024 (1983).

[10] Y. Sakuraba, J. Nakata, M. Oogane, H. Kubota, Y. Ando, A. Sakuma, and T. Miyazaki, Huge spin-polarization of $L2_1$-Ordered Co_2MnSi epitaxial Heusler alloy film, Jpn. J. Appl. Phys. **44**, L1100 (2005).

[11] L. Bainsla and K. G. Suresh, Spin polarization studies in half-metallic Co_2TiX ($X =$ Ge and Sn) Heusler alloys, Curr. Appl. Phys. **16**, 68 (2016).

[12] B. Balke, S. Ouardi, T. Graf, J. Barth, C. G. F. Blum, G. H. Fecher, A. Shkabko, A. Weidenkaff, and C. Felser, Seebeck coefficients of half-metallic ferromagnets, Solid State Commun. **150**, 529 (2010).

[13] S. Bosu, Y. Sakuraba, K. Uchida, K. Saito, T. Ota, E. Saitoh, and K. Takanashi, Spin Seebeck effect in thin films of the Heusler compound Co_2MnSi, Phys. Rev. B **83**, 224401 (2011).

[14] M. Weiler, M. Althammer, F. D. Czeschka, H. Huebl, M. S. Wagner, M. Opel, I.-M. Imort, G. Reiss, A. Thomas, R. Gross, and S. T. B. Goennenwein, Local Charge and Spin Currents in Magnetothermal Landscapes, Phys. Rev. Lett. **108**, 106602 (2012).

[15] W. Nernst, Thermomagnetische Strome, Ann. Phys. **267**, 760 (1887).

[16] K. Uchida, S. Takahashi, K. Harii, J. Ieda, W. Koshibae, K. Ando, S. Maekawa, and E. Saitoh, Observation of the spin Seebeck effect, Nature **455**, 778 (2008).

[17] J. Xiao, G. E. W. Bauer, K. Uchida, E. Saitoh, and S. Maekawa, Theory of magnon-driven spin Seebeck effect, Phys. Rev. B **81**, 214418 (2010).

[18] M. Schmid, S. Srichandan, D. Meier, T. Kuschel, J.-M. Schmalhorst, M. Vogel, G. Reiss, C. Strunk, and C. H. Back, Transverse Spin Seebeck Effect versus Anomalous and Planar Nernst Effects in Permalloy Thin Films, Phys. Rev. Lett. **111**, 187201 (2013).

[19] D. Qu, S. Y. Huang, J. Hu, R. Wu, and C. L. Chien, Intrinsic Spin Seebeck Effect in Au/YIG, Phys. Rev. Lett. **110**, 067206 (2013).

[20] L. Gravier, S. Serrano-Guisan, F. Reuse, and J.-P. Ansermet, Thermodynamic description of heat and spin transport in magnetic nanostructures, Phys. Rev. B **73**, 024419 (2006).

[21] N. Liebing, S. Serrano-Guisan, K. Rott, G. Reiss, J. S. Langer, B. Ocker, and H. W. Schumacher, Tunneling magnetothermopower in magnetic tunnel junction nanopillars, Phys. Rev. Lett. **107**, 177201 (2011).

[22] M. Hatami, G. E. W. Bauer, Q. Zhang, and P. J. Kelly, Thermal Spin-Transfer Torque in Magnetoelectronic Devices, Phys. Rev. Lett. **99**, 066603 (2007).

[23] H. Yu, S. Granville, D. P. Yu, J.-Ph. Ansermet, Evidence for Thermal Spin-Transfer Torque, Phys. Rev. Lett. **104,** 146601 (2010).

[24] M. Walter, J. Walowski, V. Zbarsky, M. Menzenberg, M. Menzenberg, M. Schefers, D. Ebke, G. Reiss, A. Thomas, P. Peretzki, M. Seibt, J. S. Moodera, M. Czerner, M. Bachmann, and C. Heiliger, Seebeck effect in magnetic tunnel junctions, Nat. Mater. **10,** 742 (2011).

[25] T. An, V. I. Vasyuchka, K. Uchida, A. V. Chumak, K. Yamaguchi, K. Harii, J. Ohe, M. B. Jungfleisch, Y. Kajiwara, H. Adachi, B. Hillebrands, S. Maekawa, and E. Saitoh, Unidirectional spin-wave heat conveyer, Nat. Mater. **12,** 549 (2013).

[26] G. E. W. Bauer, E. Saitoh, and B. J. van Wees, Spin caloritronics, Nat. Mater. **11,** 391 (2012).

[27] H. Yu, S. D. Brechet, and J.-P. Ansermet, Spin caloritronics, origin and outlook, Phys. Lett. A **381,** 825 (2017).

[28] A. Slachter, F. L. Bakker, and B. J. van Wees, Anomalous Nernst and anisotropic magnetoresistive heating in a lateral spin valve, Phys. Rev. B **84,** 020412 (2011).

[29] S. L. Yin, Q. Mao, Q. Y. Meng, D. Li, and H. W. Zhao, Hybrid anomalous and planar Nernst effect in permalloy thin films, Phys. Rev. B **88,** 064410 (2013).

[30] A. von Bieren, F. Brandl, D. Grundler, and J.-P. Ansermet, Space- and time-resolved Seebeck and Nernst voltages in laser-heated permalloy/gold microstructures, Appl. Phys. Lett. **102,** 052408 (2013).

[31] R. Ramos, M. H. Aguirre, A. Anadón, J. Blasco, I. Lucas, K. Uchida, P. A. Algarabel, L. Morellón, E. Saitoh, and M. R. Ibarra, Anomalous Nernst effect of Fe₃O₄ single crystal, Phys. Rev. B **90,** 054422 (2014).

[32] K. Hasegawa, M. Mizuguchi, Y. Sakuraba, T. Kamada, T. Kojima, T. Kubota, S. Mizukami, T. Miyazaki, and K. Takanashi, Material dependence of anomalous Nernst effect in perpendicularly magnetized ordered-alloy thin films, Appl. Phys. Lett. **106,** 252405 (2015).

[33] C. Fang, C. H. Wan, Z. H. Yuan, L. Huang, X. Zhang, H. Wu, Q. T. Zhang, and X. F. Han, Scaling relation between anomalous Nernst and Hall effect in [Pt/Co]ₙ multilayers, Phys. Rev. B **93,** 054420 (2016).

[34] T. C. Chuang, P. L. Su, P. H. Wu, and S. Y. Huang, Enhancement of the anomalous Nernst effect in ferromagnetic thin films, Phys. Rev. B **96,** 174406 (2017).

[35] M. Ikhlas, T. Tomita, T. Koretsune, M.-T. Suzuki, D. Nishio-Hamane, R. Arita, Y. Otani, and S. Nakatsuji, Large anomalous Nernst effect at room temperature in a chiral antiferromagnet, Nat. Phys. **13,** 1085 (2017).

[36] N. F. Mott and H. Jones, *The Theory of the Properties of Metals and Alloys* (New York, Dover, 1958).

[37] L. Smrčka and P. Středa, Transport coefficients in strong magnetic fields, J. Phys. C **10,** 2153 (1977).

[38] M. Jonson and G. D. Mahan, Mott's formula for the thermopower and the Wiedemann-Franz law, Phys. Rev. B **21,** 4223 (1980).

[39] W.-L. Lee, S. Watauchi, V. L. Miller, R. J. Cava, and N. P. Ong, Anomalous Hall Heat Current and Nernst Effect in the CuCr₂Se₄₋ₓBrₓ Ferromagnet, Phys. Rev. Lett. **93,** 226601 (2004).

[40] Y. Pu, D. Chiba, F. Matsukura, H. Ohno, and J. Shi, Mott Relation for Anomalous Hall and Nernst Effects in

Ga₁₋ₓMnₓAs Ferromagnetic Semiconductors, Phys. Rev. Lett. **101,** 117208 (2008).

[41] B. Ernst, R. Sahoo, Y. Sun, J. Nayak, L. Muechler, A. K. Nayak, N. Kumar, A. Markou, G. H. Fecher, and C. Felser, Manifestation of the Berry curvature in Co₂TiSn Heusler films, arXiv:1710.04393 (2017).

[42] T. Jungwirth, J. Sinova, K. Y. Wang, K. W. Edmonds, R. P. Campion, B. L. Gallagher, C. T. Foxon, Qian Niu, and A. H. MacDonald, Dc-transport properties of ferromagnetic (Ga,Mn)As semiconductors, Appl. Phys. Lett. **83,** 320 (2003).

[43] A. Akrap, A. Ubaldini, E. Giannini, and L. Forró, Bi₂Te₃₋ₓSeₓ series studied by resistivity and thermopower, EPL **107,** 57008 (2014).

[44] Z. Wang, M. G. Vergniory, S. Kushwaha, M. Hirschberger, E. V. Chulkov, A. Ernst, N. P. Ong, R. J. Cava, and B. A. Bernevig, Time-Reversal-Breaking Weyl Fermions in Magnetic Heusler Alloys, Phys. Rev. Lett. **117,** 236401 (2016).

[45] J. Kübler, G. H. Fecher, and C. Felser, Understanding the trend in the Curie temperatures of Co₂-based Heusler compounds: Ab initio calculations, Phys. Rev. B **76,** 024414 (2007).

[46] R. A. Dunlap and G. Stroink, Conduction electron contributions to the Sn hyperfine field in the Heusler alloy Co₂Ti₁₋ₓVₓSn, J. Appl. Phys. **53,** 8210 (1982).

[47] V. A. Marsocci, Magnetoresistance and Hall-voltage measurements on single-crystal Ni and Ni-Fe thin films, J. Appl. Phys. **35,** 774 (1964).

[48] S. Majumdar, M. K. Chattopadhyay, V. K. Sharma, K. J. S. Sokhey, S. B. Roy, and P. Chaddah, Transport properties of the ferromagnetic Heusler alloy Co₂TiSn, Phys. Rev. B **72,** 012417 (2005).

[49] F. C. Zumsteg and R. D. Parks, Electrical Resistivity of Nickel near the Curie Point, Phys. Rev. Lett. **24,** 520 (1970).

[50] J. M. Ziman, *Electrons and Phonons* (Oxford University Press, New York, 1960).

[51] T. Graf, G. H. Fecher, J. Barth, Jürgen Winterlik, and C. Felser, Electronic structure and transport properties of the Heusler compound Co₂TiAl, J. Phys. D: Appl. Phys. **42,** 084003 (2009).

[52] N. A. Sinitsyn, Semiclassical theories of the anomalous Hall effect, J. Phys.: Condens. Matter **20,** 023201 (2008).

[53] N. Nagaosa, J. Sinova, S. Onoda, A. H. MacDonald, and N. P. Ong, Anomalous Hall effect, Rev. Mod. Phys. **82,** 1539 (2010).

[54] I. A. Campbell and A. Fert, Transport properties of ferromagnets, Handbook Ferromagnetic Mater. **3,** 747 (1982).

[55] Y. Q. Zhang, N. Y. Sun, R. Shan, J. W. Zhang, S. M. Zhou, Z. Shi, and G. Y. Guo, Anomalous Hall effect in epitaxial permalloy thin films, J. Appl. Phys. **114,** 163714 (2013).

[56] Y. Q. Zhang, N. Y. Sun, W. R. Che, R. Shan, and G. Y. Guo, Origin of enhanced anomalous Hall effect in ultrathin Pt/permalloy bilayers, AIP Adv. **6,** 025214 (2016).

[57] J. Moritz, B. Rodmacq, S. Auffret, and B. Dieny, Extraordinary Hall effect in thin magnetic films and its potential for sensors, memories and magnetic logic applications, J. Phys. D: Appl. Phys. **41,** 135001 (2008).

[58] D. Xiao, Y. Yao, Z. Fang, and Q. Niu, Berry-Phase Effect in Anomalous Thermoelectric Transport, Phys. Rev. Lett. **97,** 026603 (2006).

[59] S. Onoda, N. Sugimoto, and N. Nagaosa, Quantum transport theory of anomalous electric, thermoelectric, and thermal Hall effects in ferromagnets, Phys. Rev. B **77,** 165103 (2008).

[60] G. Sharma, C. Moore, S. Saha, and S. Tewari, Nernst effect in Dirac and inversion-asymmetric Weyl semimetals, Phys. Rev. B **96,** 195119 (2017).

[61] B. Balke, G. H. Fecher, H. C. Kandpal, C. Felser, K. Kobayashi, E. Ikenaga, J. J. Kim, and S. Ueda, Properties of the quaternary half-metal-type Heusler alloy $Co_2Mn_{1-x}Fe_xSi$, Phys. Rev. B **74,** 104405 (2006).

[62] R. Shan, H. Sukegawa, W. H. Wang, M. Kodzuka, T. Furubayashi, T. Ohkubo, S. Mitani, K. Inomata, and K. Hono, Demonstration of Half-Metallicity in Fermi-Level-Tuned Heusler Alloy $Co_2FeAl_{0.5}Si_{0.5}$ at Room Temperature, Phys. Rev. Lett. **102,** 246601 (2009).

[63] Y. Du, G. Z. Xu, E. K. Liu, G. J. Li, H. G. Zhang, S. Y. Yu, W. H. Wang, and G. H. Wu, Half-metallicity and anisotropy magnetoresistance properties of Heusler alloys $Fe_2Co_{1-x}Cr_xSi$, J. Magn. Magn. Mater. **335,** 101 (2013).

[64] Y. Sakuraba, K. Hasegawa, M. Mizuguchi, T. Kubota, S. Mizukami, T. Miyazaki, and K. Takanashi, Anomalous Nernst effect in $L1_0$-FePt/MnGa thermopiles for new thermoelectric applications, Appl. Phys. Express **6,** 033003 (2013).

[65] J. P. Heremans, M. S. Dresselhaus, L. E. Bell, and D. T. Morelli, When thermoelectrics reached the nanoscale, Nat. Nanotechnol. **8,** 471 (2013).

[66] D.-J. Kim, K.-D. Lee, S. Surabhi, S.-G. Yoon, J.-R. Jeong, and B.-G. Park, Utilization of the antiferromagnetic IrMn electrode in spin thermoelectric devices and their beneficial hybrid for thermopiles, Adv. Funct. Mater. **26,** 5507 (2016).